Supplementary text for " A Phase Separation of Active Colloidal Suspension via Quorum-Sensing"

Francis Jose*,* Shalabh K. Anand*,† and Sunil P. Singh*‡
*Department of Physics, Indian Institute Of Science Education and Research, Bhopal 462 066, Madhya Pradesh, India

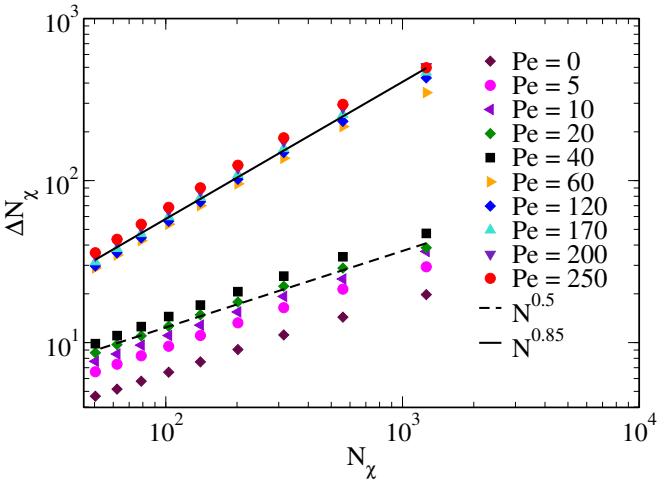

FIG. SI-1. The standard deviation ΔN_χ plotted as a function of mean number of particles N_χ for $\Phi = 0.2$. N_χ is varied by dividing the system into boxes of different sizes and calculating the mean number of particles in each box. The points are fitted according to the power-law rule.

A. Giant number fluctuations

Fluctuations become large in the phase-separated states. To quantify the fluctuations in the system, we compute the number fluctuations (ΔN_χ) in a fixed area. The equilibrium statistical fluctuations scale according to $\sqrt{N_\chi}$ for $N_\chi \to \infty$. For the self-propelled systems, it can be expressed as N_χ^ν, with ν being as large as 1 in two dimensions. Fig. SI-1 displays the estimated number fluctuations ΔN_χ as a function of the mean number of particles N_χ in an area A, which is estimated by dividing the system into subsystems of a minimum size $A = 14 \times 14$ to a maximum size of $A = 70 \times 70$. Before the onset of phase separation, ΔN_χ scales as $\Delta N_\chi \sim N_\chi^\nu$ where $\nu \approx 0.5$. In the phase-separated states, the fluctuations scale with an exponent $\nu \approx 0.85$ for all presented Pe strengths, denoting the presence of giant number fluctuations within the system. The exponent is similar to the previous studies where $\nu = 0.95 \pm 0.05$ for $\Phi > 0.4$. The large fluctuations imply that the increasing Pe leads to the growth of dense phase because of the enhancement in the collision-interactions in dense phase.

* francisjm24@gmail.com
† skanand@iiserb.ac.in
‡ spsingh@iiserb.ac.in

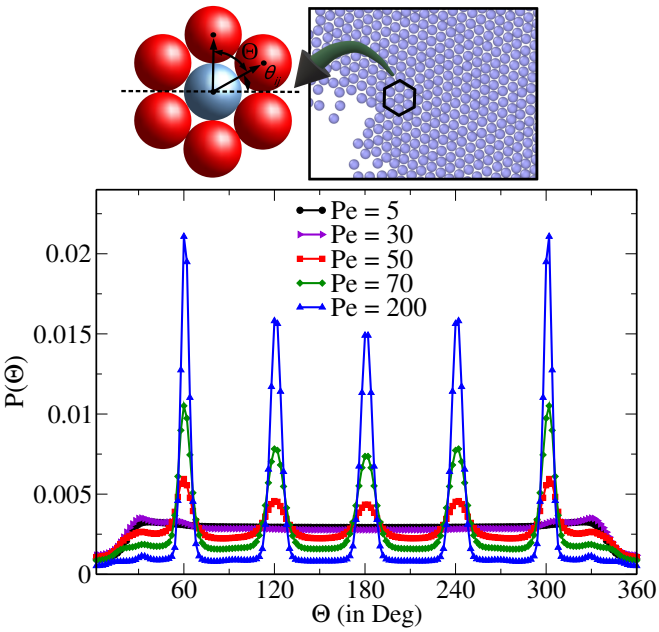

FIG. SI-2. The distribution of Θ between vectors connecting centres of particles to its six nearest neighbors at $\Phi = 0.20$. The plot shows sharp peaks at $\Theta = 60$, 120, 180, 240, and 300 for Pe beyond the transition point, where the clustered phase develops hexagonal ordering. The definition of different angles used in the analysis of the ordered phase is illustrated above.

B. Hexagonal ordering

To quantify the internal structure and its ordering in 2D, we analyse an average angle Θ (illustrated in Fig. SI-2) between two successive bond vectors connecting its six nearest neighbors around each particle. For Pe without phase separation, a flat distribution with no sharp peak indicates a phase without long-range ordering. As anticipated, sharp peaks in the distribution of Θ spontaneously appear in Fig. SI-2 at $\Theta = 60$, 120, 180, 240, and 300 for $Pe > Pe_c$, signifying hexagonal ordering.

To further analyse the structure of the cluster, analogous to Ψ_6, we employ another parameter expressed in terms of q_6 as

$$C_{q_6}(i) = \mathbf{R}e\left[\frac{1}{6}\sum_{j\in\mathcal{N}(i)} q_6(i)q_6^*(j)\right], \qquad (1)$$

where C_{q_6} can be read as an average correlation of the local order from its six nearest neighbors. This quantity

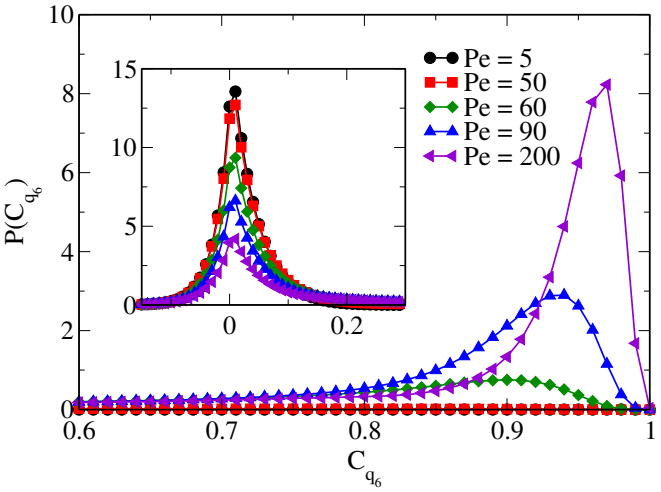

FIG. SI-3. The distribution of, C_{q6}, correlation of q_6 order parameter, plotted for various Pe. The bimodal nature of the curves above Pe $\approx$ 60 in the plot indicates appearance of localised hexagonal ordering in the clustered phase after phase separation. The distribution close to $C_{q_6} = 1$ having a prominent peak for Pe $>$ 60 confirms hexagonal close packing at $\Phi = 0.2$.

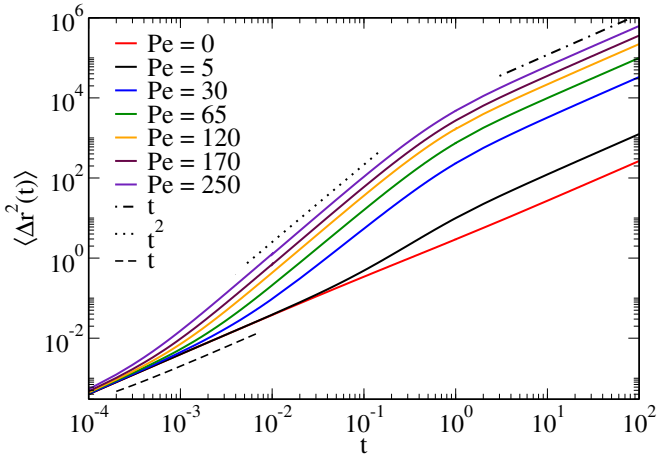

FIG. SI-4. The mean-square-displacement of all the particles in the system for various Pe at a given $\Phi = 0.2$, for $N = 5041$. The dotted line shows super-diffusive (t^2) and dotted-dashed line (long-time) and dashed line (short-time) show diffusive behavior (t).

pertains more information than Ψ_6 and can pin point the ordered and disordered phases accurately at local scale in the system. The distribution of C_{q_6} exhibits a sharp peak centred at 0 below the transition point for the homogeneous structure (see Fig. SI-3). In addition, a peak close to 1 also appears beyond the transition Péclet number confirming our claim of the hexagonal ordering. In the homogeneous phase, Ψ_6 is very small, and it always has a peak at lower values while the phase-separated states have a bi-modal behavior with a peak near $C_{q_6} \approx 1$ (see Fig. SI-3).

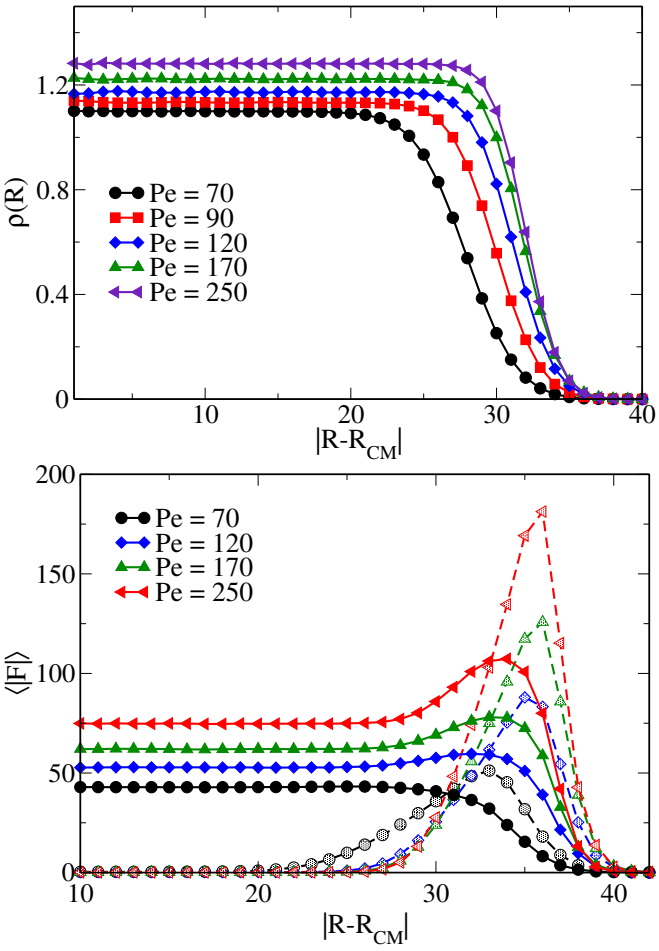

FIG. SI-5. a) The spatial variation of density of the cluster as a function of radial distance $|R - R_{CM}|$ form its centre of mass at $\Phi = 0.20$. b) The average magnitude of the repulsive force F_{LJ} (filled symbols) and the active force F_a (shaded symbols) on the largest cluster as a function of distance from the centre-of-mass $|R - R_{CM}|$ of the cluster for various Péclet numbers at $\Phi = 0.20$

C. Mean-square-displacement

Fig. SI-6 shows the MSD of the colloids averaged over all the particles in the system. The MSD of the active colloids exhibits diffusive-regime (short-time), a crossover from diffusive to ballistic behavior $\langle \Delta r^2(t) \rangle \sim t^2$ at intermediate time scales and long-time diffusive behavior with $\langle \Delta r^2(t) \rangle \sim t$. The effective diffusion coefficient is obtained from the long-time diffusive regime of Fig. SI-4.

D. Force distribution

The local density $\rho(R)$ of the largest cluster w.r.t. the distance from its centre-of-mass is displayed in Fig. SI-5-a. The density near the centre remains constant while it falls sharply towards the edge of the cluster, hence providing an estimate of the average radius of cluster.

The density falls sharply for higher Pe near the boundary, suggesting relatively weak fluctuations in its shape. The density near the centre increases with Pe, which is because of the higher crystalline ordering, a decrease in the defect density and softness of the LJ potential. The quantification of various physical forces responsible for a stable cluster with the crystalline structure is analysed in Fig. SI-5-b. The force on the largest cluster w.r.t. the distance from its centre of mass (R_{CM}) is presented here with an assumption of a spherically symmetric cluster. The magnitude of total repulsive and active forces on the largest cluster is displayed in Fig. SI-5-b.

The magnitude of repulsive LJ force is constant deep inside the cluster, and it slowly dies towards the effective boundary. The plateau value of the repulsive force in the bulk of the cluster grows with Pe as a consequence of much denser structure at high Pe. The density of particles in the outer region is small, hence the magnitude of repulsive force from the nearest interactions yields a small force in the magnitude (see Fig. SI-5)-a. For $\mathrm{Pe} > \mathrm{Pe}_c$, a peak appears near the boundary as the figure illustrates for parameter $\mathrm{Pe} \geq 120$ at $|\mathrm{R}-\mathrm{R}_{CM}| \approx 33\sigma$, and $\Phi = 0.2$. The height of peak grows very prominently with Pe. The peak in the repulsive force can be explained by the magnitude of the self-propulsive force on the surface. The active force is shown in the same plot with shaded symbols (see Fig. SI-5-b). The curve for the self-propulsion force exhibits a maxima at the surface, and it dies far from the boundary and deep inside the cluster. The behavior is along the line of our assumption that active force remains zero at higher local density, and it exhibits relatively higher active force at the edge of the cluster where it has relatively fewer neighbors.

The internal pressure of the cluster is balanced from the active force imparted by the surface molecules. As a result, a stable active crystalline phase emerges even at very small densities beyond the transition point Pe_c. For $\mathrm{Pe} < \mathrm{Pe}_c$, the difference in the average force F_{LJ} and F_a' is small; therefore, entropic force dominates over the effective attraction provided by active force. Hence, fluctuations at the boundary are dominant over the inward attraction before Pe_c.

E. Local Swim Speed

Further, we present the local swim speed to display microscopic behavior of the system's speed as a function of local packing fraction Φ_l. The swim speed, as a function of local packing fraction, is computed by dividing the system into smaller subsystems. Figure SI-6 shows the local swim speed for various Pe. The speed decreases with Φ_l. They follow a similar trend to their globally averaged counterpart illustrated in the main text. A solid line shows fitted linear function $v/v_0 = (1 - a_q\Phi_l)$ with $a_q = 1.25$. The slope obtained here is slightly smaller than the global speed. The presented local speed is slightly smaller than the global speed at the same Φ.

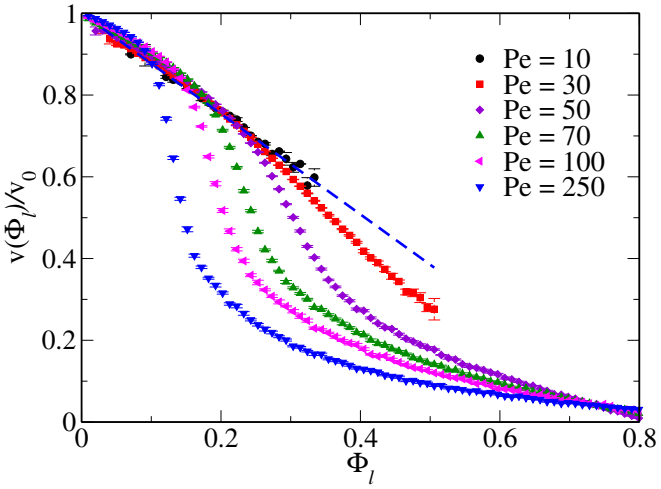

FIG. SI-6. The local directed swim speed as a function of the local packing fraction Φ_l, estimated in the subsystem of size 6×6. The dashed line represents a linear curve following the trend $v(\Phi) = v_0(1 - a_q\Phi)$ with $a_q = 1.25$

Nonetheless, the local speed essentially captures all the qualitative features of global speed for the shown Pe. Additionally, the linear-regime displays a steeper slope than generic ABP models [1–3].

F. Phase-separation without excluded volume interactions

We have also performed simulations in the absence of excluded-volume interaction. We observe that the system phase-separates even in the absence of excluded-volume interactions. This can be understood from Fig. SI-7-a, where giant Number fluctuations in systems without excluded volume interactions at $\Phi = 0.2$ and screening length for the quorum sensing $R_c = 1.3$ is plotted. The system exhibits large number fluctuations with a crossover from $N^{0.5}$ for Pe without clustering and $N^{0.8}$ for the Pe which exhibits a phase-separation. However, phase separation appears at $\mathrm{Pe}_c = 25$ for these parameters which is lower than the systems with excluded volume interactions. This is due to accumulation of larger number of particles in small sub-volume in absence of excluded-volume interactions. These clustered phases does not pertain long range hexagonal ordering, which is apparent from snapshots in Fig. SI-7-b. Further, we have done a systematic study of the influence of the choice of R_c. We find that for $R_c = 1, 1,$ 1.2, 1.3, 1.4, 1.5, and 1.6, $\mathrm{Pe}_c = 40 \pm 5$, 30 ± 5, 25 ± 5, 22 ± 2, 18 ± 2, and 16 ± 2, respectively.

G. Exponential Screening

So far, the discussion is for a linearly decaying self-propelled force on local density. In order to compare from

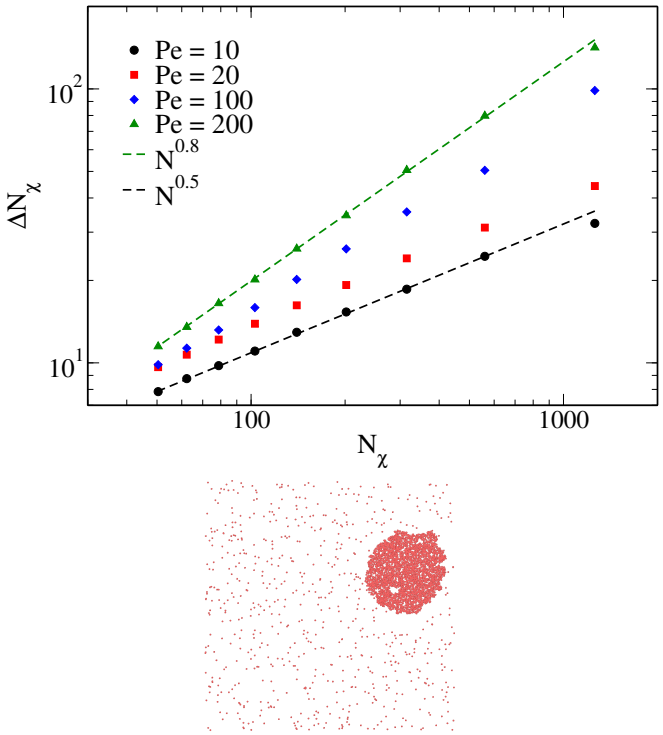

FIG. SI-7. a) Giant Number fluctuations in systems without excluded volume interactions at $\Phi = 0.2$ and screening length for the quorum sensing $R_c = 1.3$. b) Snapshot showing phase separation in systems without excluded volume interactions at Pe $= 200$, $\Phi = 0.2$ and $R_c = 1.3$.

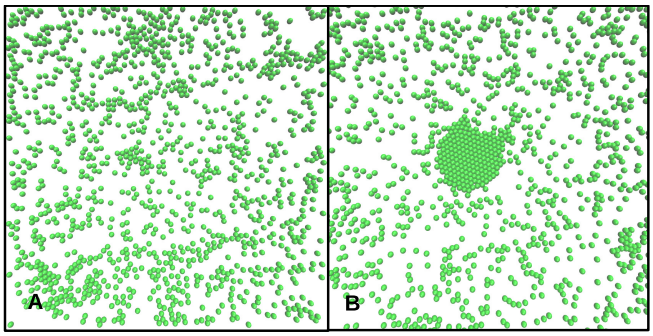

FIG. SI-8. Top: Snapshots for the system with exponential screening of active force at A) Pe $= 30$ and B) P$e = 350$ respectively for $\Phi = 0.2$.

different types of function, we choose the active force as function of its neighbors according to an exponentially decaying function given as,

$$F_{a,i}^{'} = \begin{cases} F_a & \text{if } n \leq 2. \\ \mu F_a \left(1 - \dfrac{\phi_i}{\phi_m}\right) e^{\frac{\phi_i}{\phi_m}} & \text{if } 2 < n \leq 6. \end{cases} \quad (2)$$

Here n is the number of particles lie within a cut-off radius ($R_c = 1.3$), which is kept same as that for the linear screening scheme given in the manuscript, and $F_{a,i}^{'}$ is the modified activity. We assume that when $n \leq 2$ there will be no change in the self-propulsion speed. The speed will be screened only beyond $n > 2$. A prefactor, $\mu \approx 1.031$ has been added to the quorum sensing equations so that the exponential relation would give $F_{a,i}^{'} = F_a$ when $n = 2$ and $F_{a,i}^{'} = 0$ for $n \geq 6$.

As evident, from Fig. SI-8-a and b, the cluster size does not reach the same size as that of the linear screening case. Nevertheless, the phase-separation does occur irrespective of the choice of screening function which is evident from the presence of the large aggregate. The distribution curves for higher Pe demonstrates a bi-modal curve, which spontaneously appears at the threshold Péclet number suggesting the coexistence of the two different phases. At larger Pe > 100, the peaks height near 1 becomes more prominent suggesting appearance of the hexagonal ordering at large Pe even for different model for the quorum-sensing function.

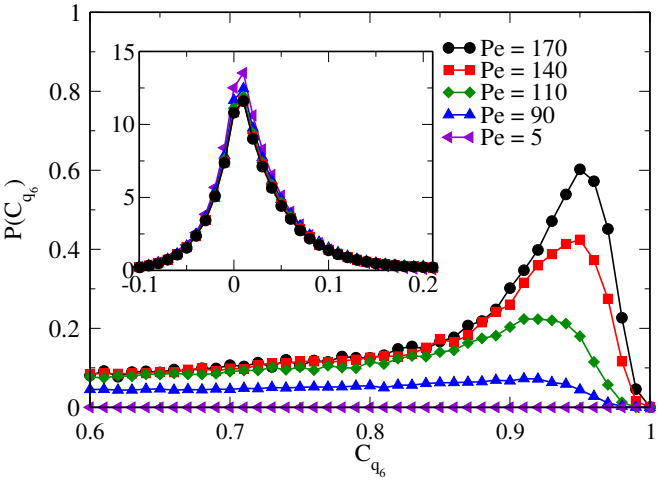

FIG. SI-9. The distribution of correlation function of q_6 vector, C_{q_6} for various Péclet numbers. The bi-modal nature of the curves above Pe ≈ 60 indicates phase separation.

H. Supporting Movie files

1. SI - Movie-1: The movie shows the dynamics of the active colloids in the phase-separated states. The color of colloid illustrates number of nearest neighbors, here red for n=6, green is $n = 5$, and blue for $n < 5$, at $Pe = 70$ and $\Phi = 0.2$.

2. SI - Movie-2: The movie shows the dynamics of the active colloids in the phase-separated states. The color of colloid illustrates number of nearest neighbors here red for n=6, green for $n = 5$, and blue for $n < 5$, at $Pe = 100$ and $\Phi = 0.2$.

[1] J. Stenhammar, D. Marenduzzo, R. J. Allen, and M. E. Cates, Soft matter **10**, 1489 (2014).
[2] J. Stenhammar, A. Tiribocchi, R. J. Allen, D. Marenduzzo, and M. E. Cates, Physical review letters **111**, 145702 (2013).
[3] Y. Fily and M. C. Marchetti, Physical review letters **108**, 235702 (2012).